Superconducting THz Detectors and Their Applications in Radio Astronomy

Sheng-Cai SHI
Purple Mountain Observatory, National Astronomical Observatories, Chinese Academy of Sciences, Nanjing 210008, China
scshi@pmo.ac.cn

doi: 10.11906/TST.190-206.2008.12.16

1. Introduction

It is common knowledge now that the THz region, loosely defined from 0.1 *THz* to 10 *THz*, is rich in scientific and technological opportunities. For example, THz astronomical observations may help answer key questions in the field of astronomy and cosmology. In fact, an entirely new class of galaxy, formed at a very early stage in the universe, has recently been discovered through THz observations [1]. The THz region, however, is to be fully explored as technologies available for this frequency regime are still rather limited. One of significant technical challenges is the development of THz detectors of high sensitivity and large array sizes.

As is well known, detectors can be classified into two categories: incoherent detectors (namely direct detectors, e.g., bolometer) and coherent detectors (e.g., heterodyne mixers). The former is typically of large bandwidth and low or moderate spectral resolution mainly characterizing thermal emissions, while the latter of small bandwidth and high spectral resolution mainly characterizing molecular and atomic spectral lines. On the other hand, superconducting detectors, based essentially on the mechanism of Cooper-pair breaking, have very high sensitivity and can be developed for large arrays (multiple pixels) through lithographic fabrication. They are finding widely used in the fields ranging from astronomy to biology and medicine [2-3].

In this paper, we mainly introduce the major work which was exactly done in sub-millimeter laboratory of Purple Mountain Observatory (PMO). There are four chief aspects:

1) Nb superconducting SIS mixers;

2) NbN superconducting SIS mixers;

3) phonon-cooled superconducting HEB mixers;

4) direct detection with SIS junctions.

2. Nb Superconducting SIS Mixers

We have developed superconducting SIS receivers at the frequencies of 100-, 500- and 660-GHz. Here we would like to take the 500-GHz one for instance, which was developed for the portable submillimeter telescope (POST) to observe the 492GHz line of neutral atomic carbon (CI) along the galactic plane [4]. Taking account of that distributed junction arrays, which are a number of SIS junctions connected in parallel with every two junctions separated by a tuning inductance, have large band width even with low-J_c SIS junctions [5-6], we investigated the 500-GHz waveguide superconducting SIS mixer with a five junction array.

The drawing of the SIS junction chip mounted inside the mixer block is shown in Fig. 1, together with the photograph of the distributed junction array. The 500-GHz waveguide SIS mixer had a half-reduced height

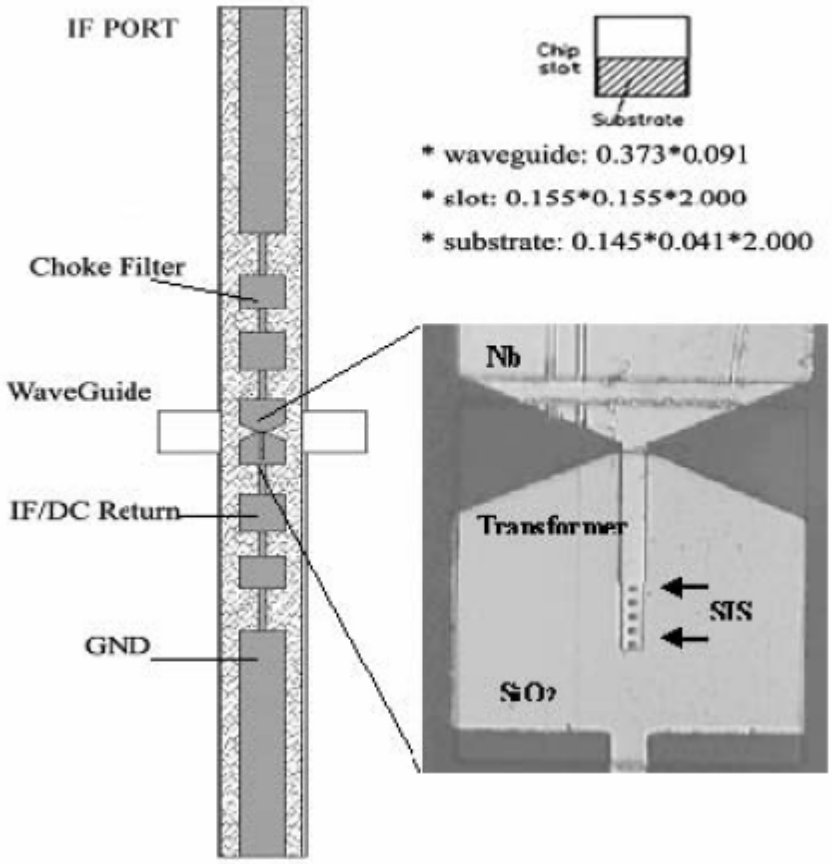

Fig.1 Drawing of the SIS junction chip and the photograph of the distributed junction array composed of five junctions.

waveguide measuring 373μm*91μm, making impedance matching easier. The junction feed point, which coupled RF and LO signals to the distributed SIS junction array, was located right at the waveguide center. The distributed junction array had five identical Nb/AlOx/Nb SIS junctions

that were designed to have an area and critical current density of 1.21μm^2 and 10kA/cm^2, respectively, corresponding to a normal state resistance of 16.12 Ω (i.e., 3.22 Ω for the five junction array). The tuning inductances in between two individual SIS junctions were also identical, i.e., 5-μm wide and 4.4-μm long thin film superconducting microstrip line that was composed of Nb (0.6μm)/SiO_2 (0.25μm)/Nb (0.2μm) three layers. An impedance transformer was placed in between the junction feed point and the five junction array for impedance matching. The RF embedding impedance of the 500-GHz waveguide SIS mixer, seen at the junction feed point, was computed with the aid of HFSS in the frequency range of 450-650 GHz. The results are plotted on a Smith impedance chart (see Fig. 2). The embedding impedance at 500 GHz is 26.6-j38.1Ω ,and it becomes 1.3-j3.0Ω ,after the impedance transformer.

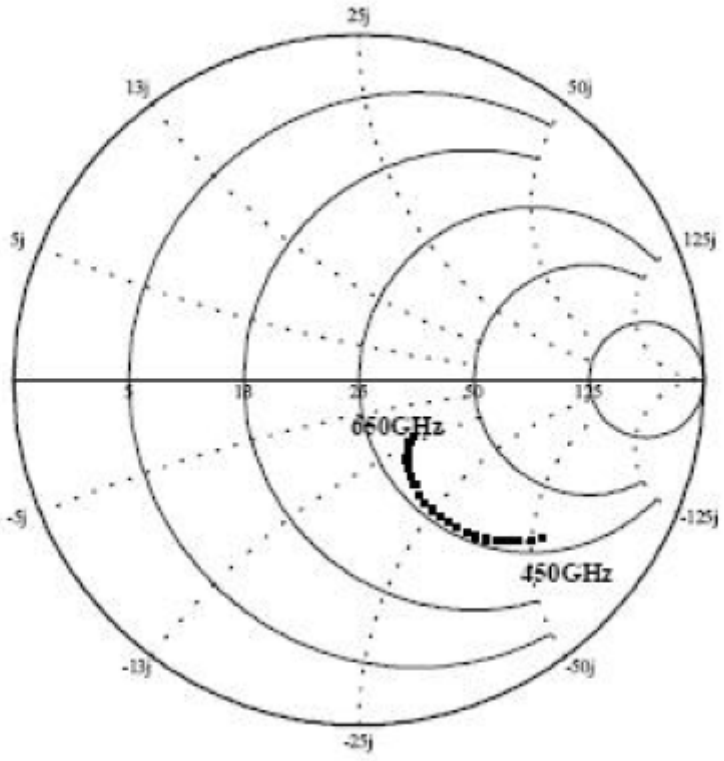

Fig.2 Embedding impedance seen at the junction feed point(Z_{emb}),plotted on a smith impedance chart.

For testing the performance, a quasi-optical system, which is indeed just a simple beam splitter made of thin Mylar film, combines the RF and LO signals at an angle of 45 degrees relative to the incident directions of both signals. The RF signal is hot/cold blackbody source, while the LO source a combination of an 83-GHz Gunn oscillator and a 6-time multiplier. The IF output signal of the SIS mixer was firstly amplified by the 1.2-1.8 GHz HEMT amplifier, then further amplified by a room temperature amplifier and filtered by a band-pass filter of 1.65±0.087 GHz. We recorded the IF output signal using a direct detector of a detection sensitivity of 1mV/μW. The DSB receiver noise temperature of the 500-GHzwaveguide SIS mixer was measured using the standard Y-factor method. Fig. 3 demonstrates typical I-V and P_{IF}-V characteristics of the waveguide SIS mixer measured at 500GHz. It should be pointed out that in this case, the

quasi-optical system was already optimized for its transmission efficiency and beam width coverage. The photon assisted tunneling step looks fairly flat (i.e., of a large dynamic resistance), indicating high mixer conversion gain. Moreover, a dip can be found around 1.5mV, which is indeed due to the effect of the second photon-assisted tunneling step originated from the negative gap voltage. We did the noise temperature measurement for the beam splitter of different Mylar-film thicknesses (15- and 36-μm), different locations from the waveguide SIS mixer, and different LO-source incidence modes (TE and TM mode) to understand the noise contribution of the quasi-optical system. The calculated reflection and transmission around 500 GHz for four cases of the beam splitter are plotted in Fig. 4. Obviously, the thinner the Mylar film, the larger the signal transmission is. And the TE mode incidence has larger reflection than the TM mode incidence.

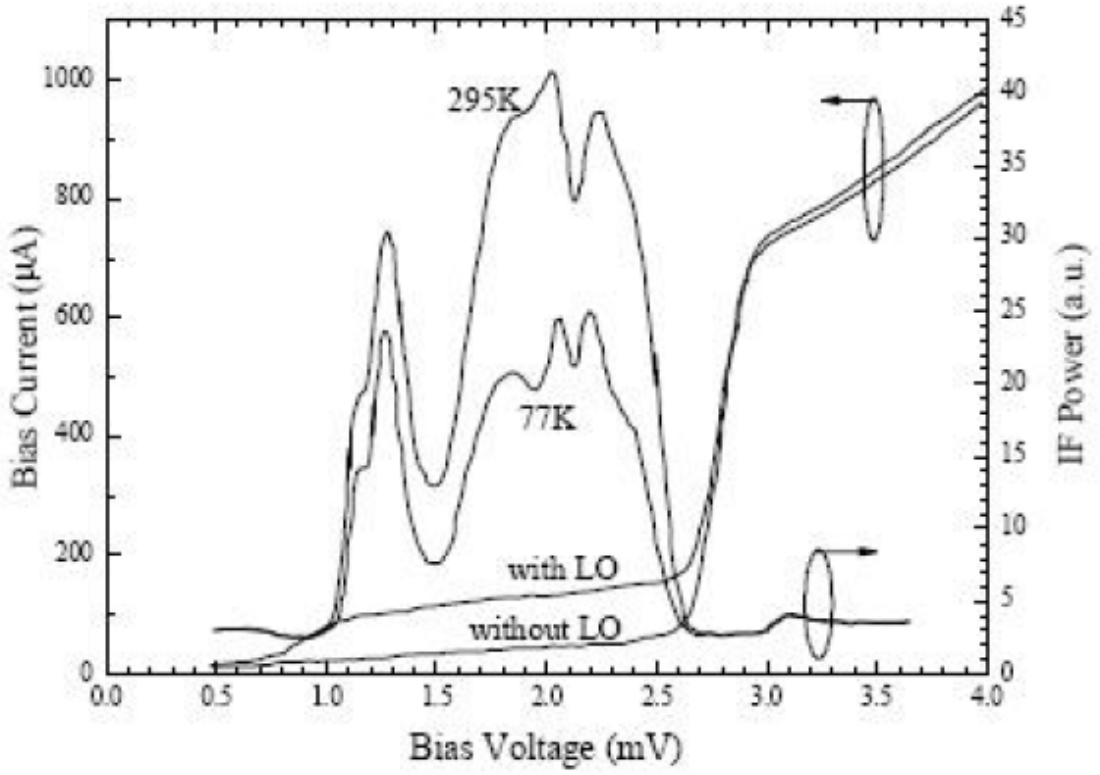

Fig.3 Measured junction I-V characteristics with and without LO pumping at 500 GHz. Also shown is the IF output power as a function of bias voltage corresponding to the hot (295K) and cold (77K) loads. The maximum Y factor is recorded at 1.9 mV.

3. NbN Superconducting SIS Mixers

As mentioned above, SIS mixers with Nb/AlOx/Nb junctions have achieved noise temperatures as low as three times the quantum limit below 0.7THz, which is the gap frequency of Nb SIS junctions [7]. However, at frequencies higher than 0.7THz, the transmission loss in an Nb microstrip line increases significantly due to the breaking of cooper pairs, thereby

deteriorating the noise performance of Nb SIS mixers obviously. Therefore high energy-gap superconducting materials, such as niobium nitride (NbN), are required for developing SIS mixers at frequencies beyond 0.7THz.

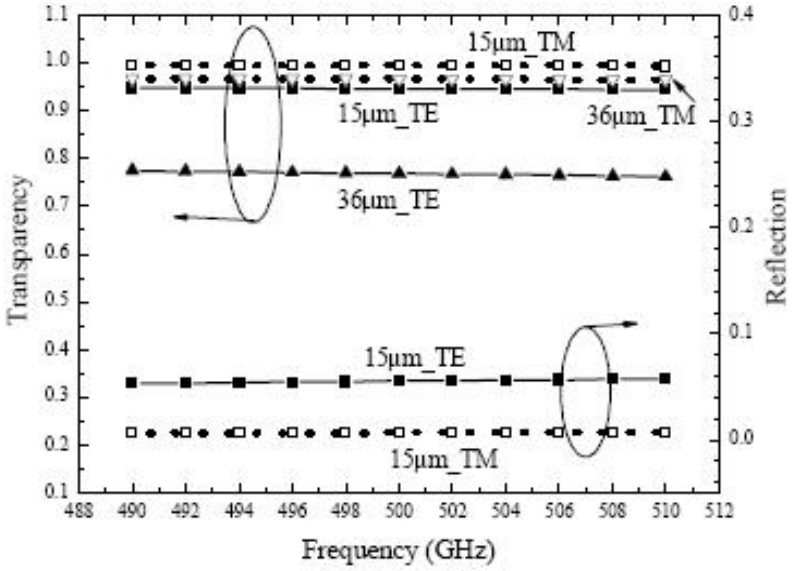

Fig.4 Transmission of Mylar films of different thicknesses; also shown is the reflectivity of a 15-m thick Mylar film with the TE- and TM-mode incidence.

Single-crystal NbN films fabricated on an MgO substrate have a high superconducting energy gap, which is corresponding to a gap frequency of about 1.4 *THz*. Considering the bandwidth and output power of local-oscillator (LO) signal sources are quite limited beyond and even around 1 *THz*, we firstly develop a waveguide NbN-based SIS mixer at 0.5 *THz* as a scale model for demonstrating the good performance of NbN SIS junctions. Here we mainly focus on the fabrication process, and the preliminary FTS performance and noise temperature measurement results.

For the fabrication of all-NbN SIS junctions, we used the conventional method of lithography. Firstly, the tri-layer of NbN/AlN/NbN was deposited an a single-crystal MgO substrate without additional substrate heating. The NbN films were prepared by reactive dc-magnetron sputtering, and relative amounts of argon and nitrogen introduced for sputtering were controlled by mass flow controllers. To promote the growth of NbN films at low substrate temperatures, a low total pressure and high power density were used for depositing the films [8]. The AlN barrier was also deposited by dc sputtering. In order to control the barrier thickness and the temperature rise of the MgO substrate, the AlN film was deposited in pure N2 gas at a low-power density. The thickness of the thin film barrier determines the critical current density (J_c) of the SIS junctions. Some of the sputtering parameters are listed in Table. 1.

After tri-layer sputtering, the waveguide probe and choke filter were formed by photolithography, and then etched by reactive ion etching (RIE) with CF_4 (for NbN) and Ar (for AIN) gases. Secondly, the SIS junctions were defined and a 250-*nm* thick SiO_2 layer was deposited by RF sputtering to insulate the base and wiring electrode. After lifting off the ~700 *nm*

photo resist (AZ5206), a 350-nm thick wiring Nb layer was deposited and patterned finally. Fig.5 explains the general process, and Fig.6 shows the photo of parallel connected two junctions (PCTJs).

NbN Film		**AlN Film**	
Base pressure	<2E-5Pa	**Base pressure**	<2E-5Pa
Target clean	3min by Ar	**Target clean**	3min by Ar
Sputtering gas	Ar:100sccm N_2:38sccm	**Sputtering gas**	N2:100sccm
Total pressure	2mtorr	**Total pressure**	2mtorr
DC current	3A	**DC power**	100W
Deposition rate	~1.4nm/sec	**Deposition rate**	0.1~0.2nm/sec

Table.1 Sputtering parameters for the tri-layer of NbN/AlN/NbN.

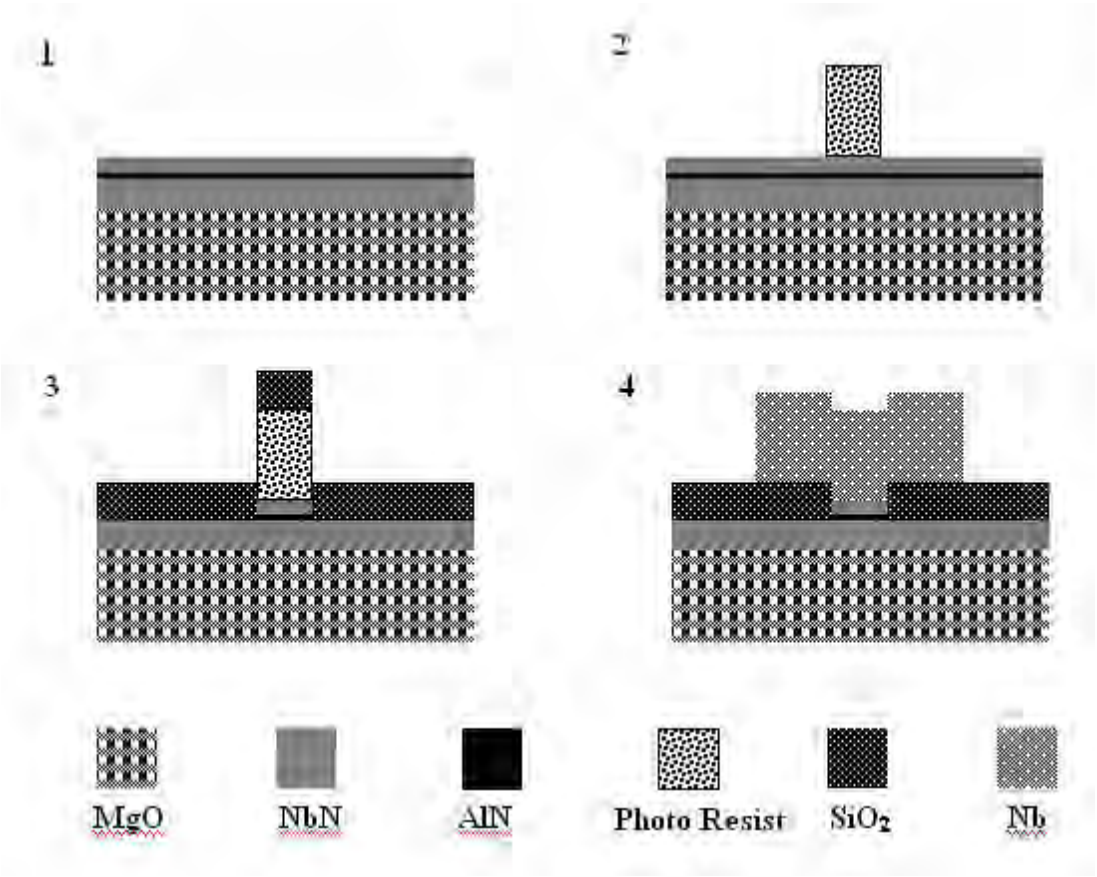

Fig.5 Fabrication process adopted in the cleanroom.

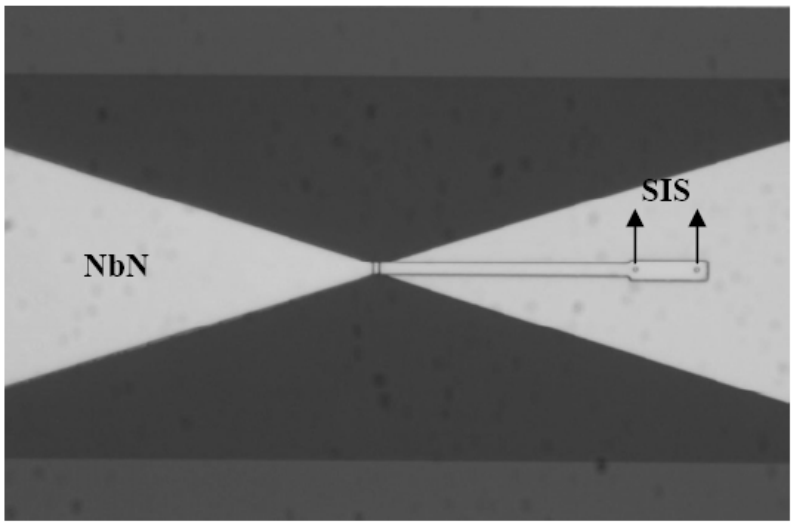

Fig.6 Photograph of the 0.5-THz NbN SIS junction chip.

We measured the direct-detection response of the 0.5-*THz* waveguide NbN SIS mixer with a Fourier Transform Spectrometer (FTS). In the testing system, vacuum was pumped to get rid of the H2O absorption line at 557 *GHz*. The 0.5-*THz* waveguide NbN SIS mixer was cooled down to 4.2 *K* by a LHe cryostat and a magnetic field was applied to suppress the Josephson effect. It was measured at two different dc bias voltages, i.e., 3.5 and 4.0 *mV*. The tested interferogram and FTS responses are demonstrated in Fig. 7. Obviously, the two curves are of pretty similar shape,

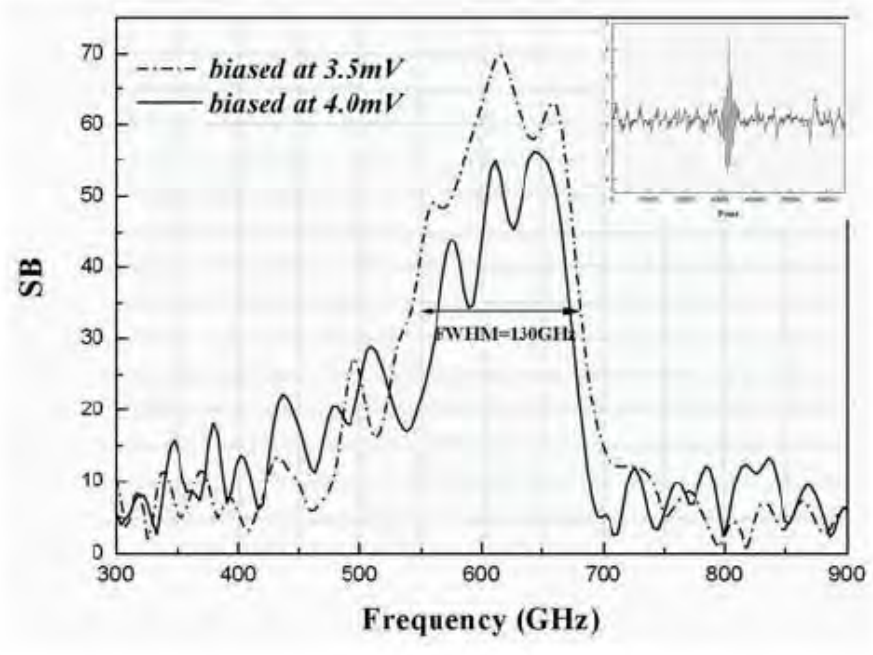

Fig.7 Measured FTS responses of the 0.5-THz waveguide NbN SIS mixer.The inset is a typical interferogram.

indicating high reproducibility of our experimental results. The center frequency was located at about 0.61 *THz* and FWHM is approximately equal to 130 *GHz*. It is clear that the center frequency of the FTS response is much higher than the designed value and the observed resonance frequency. This frequency shift might be due to the over shrinkage of the junction size.

4. Phonon-Cooled Superconducting HEB Mixers

Superconducting hot-electron bolometer (HEB) mixers are becoming the heterodyne receiver of choice for high-sensitivity and high-spectrum-resolution ($\nu/\Delta\nu>106$) detection in astronomy and atmospherid 1.5 *THz* [9]]. The noise performance of phonon-cooled superconducting NbN HEB mixers has approached ten times the quantum limit (10 $h\nu/k$) in the THz range. Another important parameter of superconducting HEB mixers is the intermediate frequency (IF) bandwidth, which needs to be sufficiently large for spectral observations since the continuous frequency tuning of THz local oscillator (LO) sources is very limited. even impossible for optically pumped far infrared gas lasers. Phonon-cooled superconducting NbN HEB mixers on the silicon substrate have a gain bandwidth of about 3 *GHz*, which can be increased to approximately 5 *GHz* with an MgO buffer layer introduced, satisfying the needs of astronomicaland atmospheric observations [10].

Here we systematically measured and analyzed the noise performance of log-spiral antenna coupled superconducting NbN HEB mixers on the bath temperature and off-axis displacement from the center of an extended hemispherical silicon lens to understand the dependence of noise temperature of superconducting NbN HEB mixers on the bath temperature and optical-axis displacement. The dependence of noise temperature of superconducting NbN HEB mixers upon the absorbed LO power is thoroughly studied by calculating the LO power requirement at the same working point but different bath temperatures with the isothermal method [11].

Log-spiral antenna coupled superconducting NbN HEB mixers were fabricated from 3.5-*nm* thick NbN film. They were simply made up of a log-spiral antenna and a superconducting NbN micro-bridge across the antenna's feed point. The superconducting NbN HEB bridge (refer to the inset of Fig.8) was defined via electron beam lithograph.

The current-voltage characteristics of the quasi-optical superconducting NbN HEB mixer were firstly measured when the bath temperature was changed by Lakeshore 340 temperature controller. As depicted in Fig. 9, the critical current of the quasi-optical superconducting NbN HEB mixer gradually drops as a result of the depression of superconductivity with the increase of the bath temperature. Since there are two transition temperatures with respect to the NbN micro-bridge and Au contact, the superconducting NbN film under Au contact firstly converted from the superconducting state into the normal state around the bath temperature of ~7 *K*, leading to the increase of residual resistance of superconducting NbN HEB device. Consequently the slope of I- V curves of the superconducting NbN HEB device at bias voltages below 0.5 *mV* was increased, although NbN micro-bridge was still in the superconducting state.

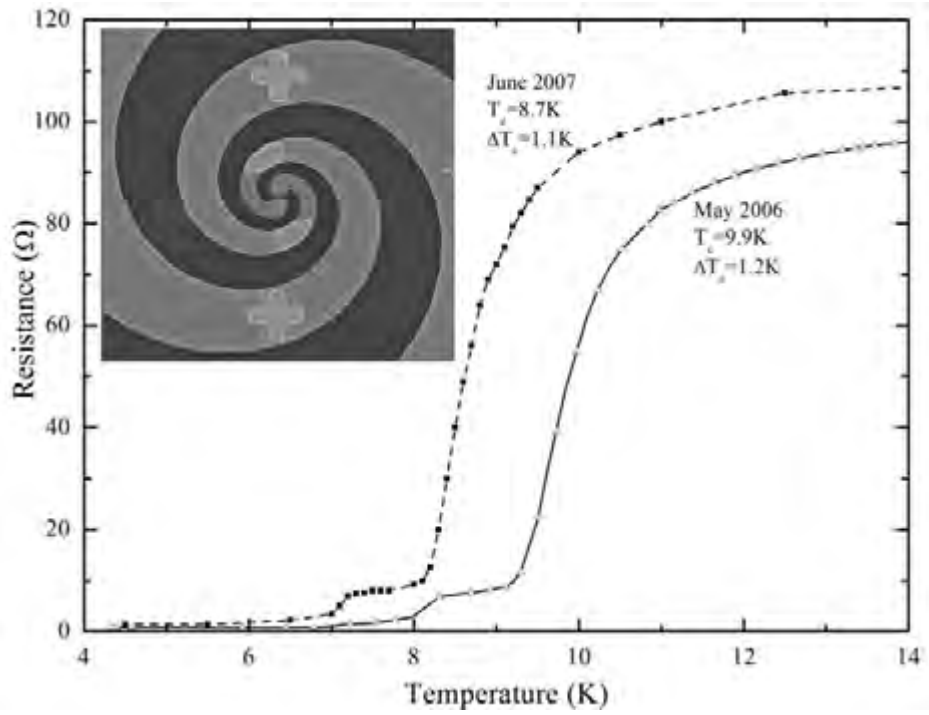

Fig. 8 Temperature dependence of resistance of the log-spiral antenna coupled superconducting NbN HEB device measured half and one year before. The inset shows a photograph of the log-spiral antenna coupled superconducting NbN HEB mixer measuring 0.32μm long and 4μm wide.

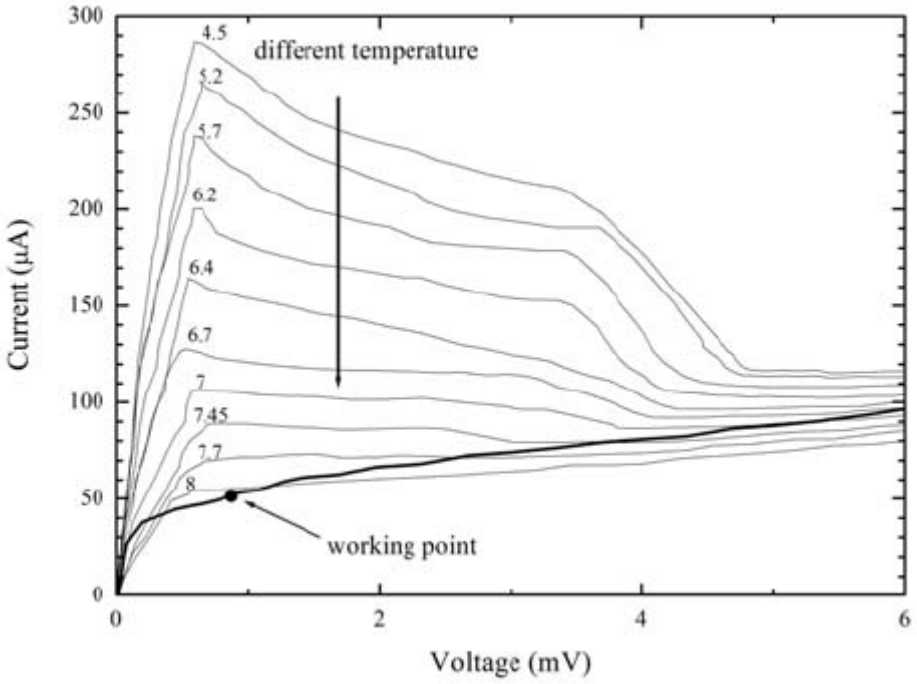

Fig.9 Current-voltage curves of the superconducting NbN HEB mixer at different bath temperatures. Also shown is the working point, where noise temperature of the superconducting NbN HEB mixer was measured.

The measured noise temperature of the quasi-optical superconducting NbN HEB mixer is 1500 *K* at 0.5 *THz* and 2000 *K* at 0.85 *THz*, which are both higher than those measured a year earlier (800 *K* at 0.5 *THz* and 1100 *K* at 0.85 *THz*) [12]. We attributed the change of noise temperature to the deterioration of quality of the 3.5-*nm* superconducting NbN film. We also measured the noise temperature at 0.5 *THz* and critical current of the quasi-optical superconducting NbN HEB mixer at different bath temperatures (4.5-8 *K*), while keeping the working point constant (V0=0.9 *mV* and I0=51 μA). The results are shown in Fig.10.

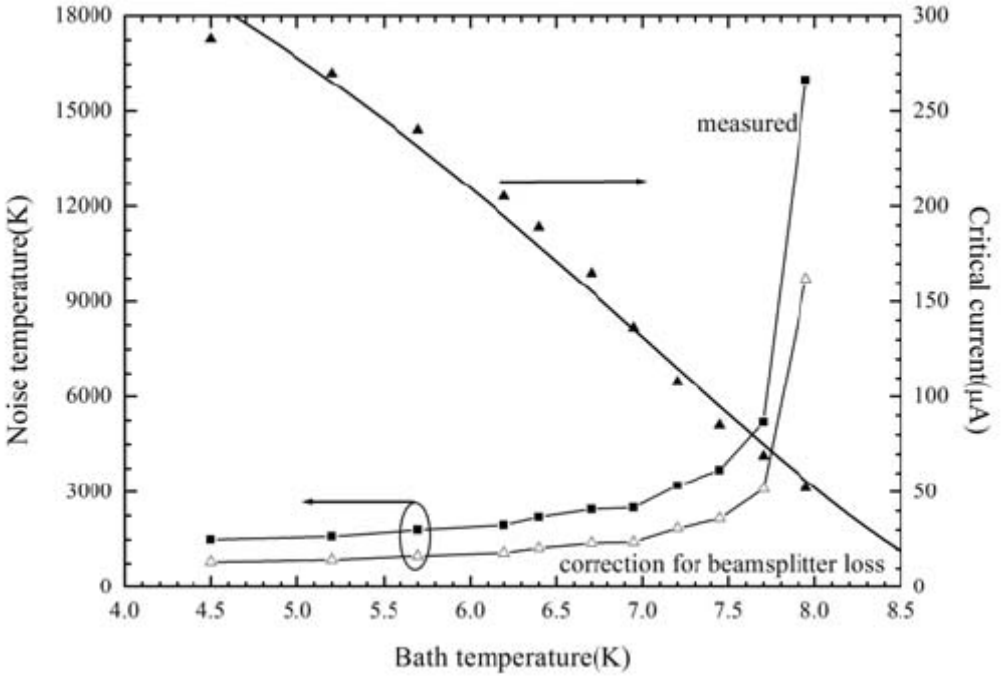

Fig.10 Noise temperature and critical current of the superconducting NbN HEB mixer as a function of bath temperature at 0.5 *THz*. Also shown is the corrected noise temperature for the transmission loss and associated noise contribution of the beamsplitter made up of a 50-μm thick Mylar film.

It can be clearly seen from Fig.10 that the noise temperature of the quasi-optical superconducting NbN HEB mixer measured at 0.5 *THz* almost remains constant below 7 *K*, but increases sharply beyond 7.5 *K*. Also shown in Fig.10 is the noise temperature of the superconducting NbN HEB mixer corrected for the transmission loss and associated noise contribution of the beam splitter made up of a 50-μm thick Mylar film. Obviously, the corrected noise temperature of superconducting NbN HEB mixer is down to 800 *K* at 4.5 *K*.

The noise temperature of superconducting NbN HEB mixers were inversely proportional to the LO power. Here we examine its validity in terms of the noise temperatures measured at different bath temperatures. As shown in Fig.10, we measured the noise temperature of a quasi-optical superconducting NbN HEB mixer at the same working point when the bath temperature was changed. Meanwhile, its LO power requirement was also calculated according to the isothermal model [14]. At the same working point, the absorbed DC power (V0 I_0) and DC resistance (V0/I0) of the quasi-optical superconducting NbN HEB mixer remain constant. The RF coupling between the log-spiral antenna and the superconducting NbN HEB micro-bridge is therefore constant, and

the IF coupling between the IF chain and the superconducting NbN HEB mixer is almost fixed since the differential resistance of the superconducting NbN HEB device at the same working point was found nearly nochange with the bath temperature.

It is inevitable that there exists some displacement between the measured superconducting NbN HEB device and the center of the adopted extended hemispherical silicon lens. The far-field patterns and Gaussian-beam coupling are investigated for a double-slot antenna placed off-axis on the extended hemispherical silicon and quartz lenses [15]. In order to understand the influence of optical-axis displacement on the noise temperature of the log-spiral antenna coupled superconducting NbN HEB mixer, the superconducting NbN HEB device mounted on the flat side of extended hemispherical silicon lens with a precision better than 5 μm was moved away from the center of the silicon lens in the range of 0 ~ 180 μm. Its noise temperature was measured correspondingly at 0.5 *THz*. Note that for all the measurements taken relative to the displacement the critical current of the log-spiral antenna coupled superconducting NbN HEB device remained unchanged and the working point was fixed at the optimum bias of 0.9 mV and 51 μA.

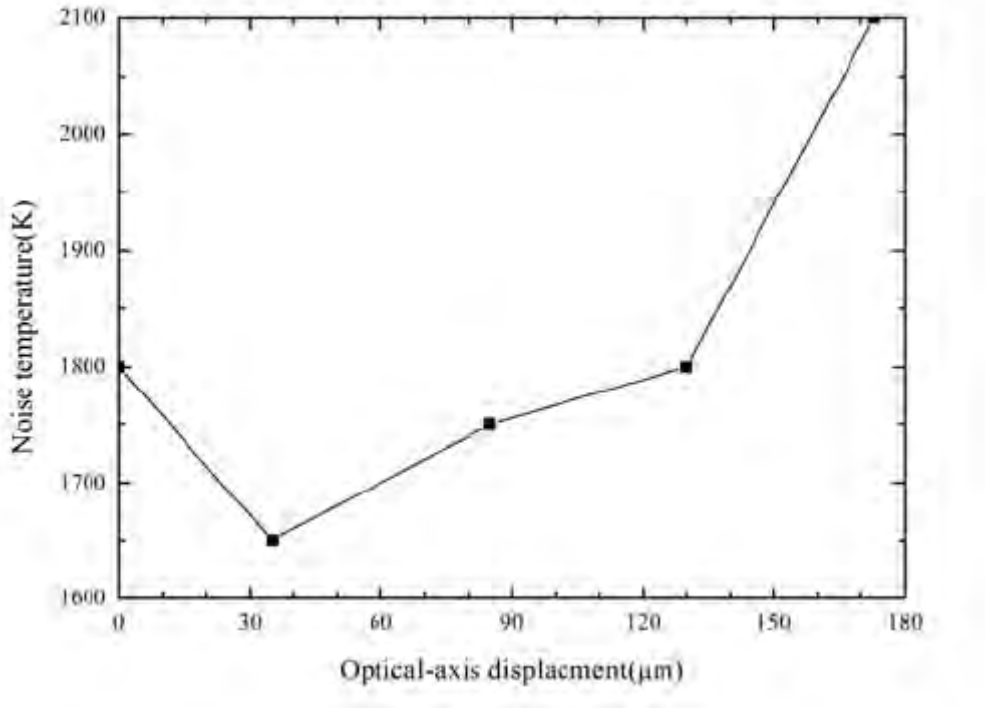

Fig.11 Noise temperature of the log-spiral antenna coupled superconducting NbN HEB mixer as a function of optical-axis displacement at 0.5 THz.

The measured noise temperature of the log-spiral antenna coupled superconducting NbN HEB mixer is shown in Fig. 11 as a function of the optical-axis displacement. Surprisingly, the minimum noise temperature appears at an optical-axis displacement of about 35μm. The noise temperature of the log-spiral antenna coupled superconducting NbN HEB mixer increases slowly when the displacement is beyond or below this value. We attribute this non-zero displacement to a lower refractive index of our silicon lens, which was designed to be a synthesized elliptical lens with a diameter of 12 *mm*. Probably the refractive index of the silicon lens was less than its nominal value of 3.42 owing to impurity, thus synthesized elliptical lens required a little more

extended length. When the superconducting NbN HEB device moved away from the center of the extended hemispherical silicon lens, equivalent to increasing the extended length, to the optimum displacement of about 35 μm, it just met the requirement of synthesized elliptical lens with a diffraction-limited beam pattern. In this case the coupling efficiency between the log-spiral antenna coupled superconducting NbN HEB device and the black body radiation was the largest, thereby giving the minimum noise temperature. With further increase of the optical-axis displacement, the side lobe of the antenna's beam pattern was increased and the coupling efficiency was decreased, thus leading to the increase of the mixer noise temperature.

5. Direct Detection with SIS Junction

Next, we mainly focus on the investigation of THz detection with twin SIS tunnel junctions that are made up of two identical Nb/AlOx/Nb junctions connected in parallel through an inductive thin-film superconducting microstrip line. Twin SIS tunnel junctions have relatively high input impedance, which is beneficial to broadband matching, and yet are of a simple structure to fabricate. At first, we measure the direct-detection response of a superconducting twin-junction device with the help of a Fourier Transform Spectrometer. We also construct a theoretical model of direct detection for twin SIS tunnel junctions. On the basis of this model, the direct-detection response of the measured superconducting twin-junction device is simulated. Its noise temperature behavior is also demonstrated for comparison.

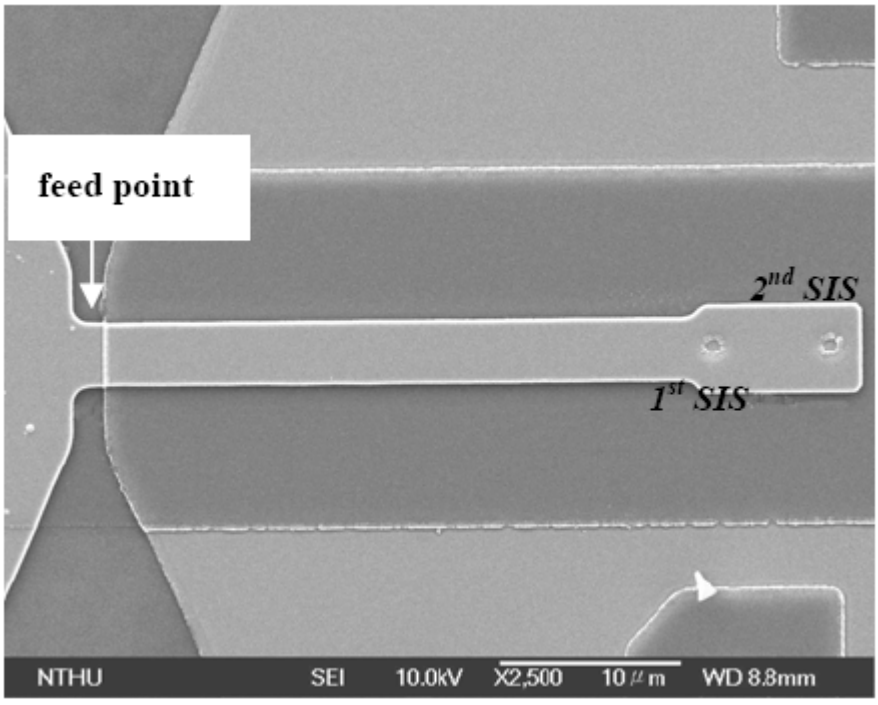

Fig.12 SEM photograph of the measured superconducting twin-junction device (mainly the center part with twi SIS junctions and superconducting microstrip lines).

As shown in Fig.12, the measured superconducting twin-junction device has two identical Nb SIS junctions separated by a thin-film superconducting microstrip line. The superconducting twin-junction device was accommodated in a waveguide mount with a corrugated feed horn [16] and then mounted in a LHe cryostat to cool it down to 4.2 *K*. Note that the device's feed point was just located at the waveguide center in order to have good coupling of THz radiation in a large bandwidth. Using an FTS system, we investigated the direct-detection response of the superconducting twin-junction device. Notice that the FTS system was vacuum-pumped to get rid of the H2O absorption line at 0.557 *THz*. The FTS system, with a mercury lamp as the radiation source, is able to cover a very large frequency range from a few GHz to approximately 240 *THz*, and yet is of high frequency resolution (~5 *GHz*). The superconducting twin-junction device had a gap voltage of about 2.75 *mV* at 4.2 *K* and was dc-biased at 2 *mV*. With such a dc-bias voltage, we could measure its direct-detection response at frequencies down to 0.18 *THz* with a relatively small dark current. In fact, it was the voltage that we characterized the heterodyne-detection performance of the superconducting twin-junction device. Fig. 13 displays the measured direct-detection response, together with its interferogram. Its center frequency is about 0.72 *THz* and FWHM is approximately 0.17 *THz*. Obviously, there is a fairly good signal-to-noise ratio. It can also be seen clearly that this detection response has no spurious responses. Strict design criteria applied to the waveguide mount might suppress high-order modes, which are usually the major cause of spurious responses.

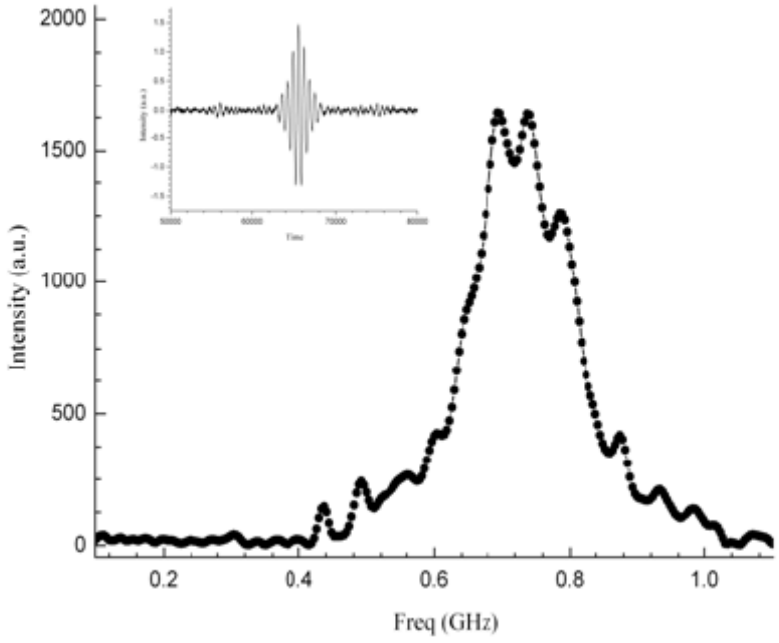

Fig.13 Measured direct-detection response of the superconducting twin-junction device (inset is shown for its interferogram).

As it is well known, the direct-detection response of a detector can be described by its intrinsic responsivity and the power coupling efficiency between the source and the device. The current responsivity (Ri), defined as the change in dc current per unit power absorbed, of a single superconducting SIS junction has already been established by Tucker [17]. Its quantum-limited

value is equal to e/hν, where e is the charge of a single electron, h Planck's constant, and ν the frequency of the absorbed photon, representing one additional electron flowing through the junction barrier for each incoming photon absorbed. When a monochromatic signal is incident on a superconducting twin-junction device from its single feed, the two SIS junctions will have different sinusoidal voltages owing to the separation between them, thereby producing different dc currents and dissipative components at the signal frequency. If the signal frequency is lower than the gap frequency of superconducting films, there will be no power dissipation along the superconducting microstrip line connecting the two SIS junctions. Given the fact that the change of dc current of a single SIS junction is linearly related to incident power for sufficiently low intensities, we can find the current responsivity of twin SIS junctions is indeed the same as that of individual SIS junctions no matter how long the separation is. If the signal frequency is higher than the gap frequency of superconducting films, there will be considerable film losses resulted from the Cooper-pair breaking by energetic photons. The current responsivity of twin SIS junctions is therefore dependent upon the characteristics of superconducting microstrip lines, besides the current responsivity of individual junctions.

Let us assume a sinusoidal voltage

$$V_2(t) = V_0 + \mathrm{Re}(V_2 e^{j\omega t}) \tag{1}$$

is impressed on the second SIS junction of a superconducting twin-junction device. Here V0 is the constant bias potential across the two SIS junctions, and ω the angular frequency of the incoming signal. The voltage developed across the first SIS junction can be written in the form

$$V_1(t) = V_0 + \mathrm{Re}(V_1 e^{j\phi} e^{j\omega t}) \tag{2}$$

where Φ is the phase shift resulted from the superconducting microstrip line between the two SIS junctions. According to the formulae derived by Tucker [17], the incremental dc currents and current components induced at the signal frequency by the two respective sinusoidal voltages are written

$$\Delta I_{dc,i} = \frac{1}{4} V_i^2 \left\{ \frac{I_{dc}\left(V_0 + \hbar\omega/e\right) + I_{dc}\left(V_0 - \hbar\omega/e\right)}{\left(\hbar\omega/e\right)^2} \right\} \tag{3}$$

$$I_{\omega,i} = V_i \, e^{j\varphi_i} \left\{ \frac{I_{dc}\left(V_0 + \hbar\omega/e\right) - I_{dc}\left(V_0 - \hbar\omega/e\right)}{2\left(\hbar\omega/e\right)} \right\} \tag{4}$$

where i=1,2, $\psi_1 = \phi$ and $\psi_2 = \phi$. Using the transmission line theory, we can obtain the voltage V1 and associated phase shift Φ in terms of the voltage V_2 and resultant current $I_{\omega,2}$

$$V_1 e^{j\phi} = \cosh \gamma l * V_2 + Z_0 \sinh \gamma l * \left(I_{\omega,2} + j\omega C_j V_2 \right) \tag{5}$$

where Cj is the geometric capacitance of individual SIS junctions, and γ and Z_0 are the

propagation constant and characteristic impedance of the superconducting microstrip line, which can be calculated by taking account of the surface impedances of the conductor strip and ground plane of the superconducting microstrip line. Similarly, the resultant current at the input port of the superconducting microstrip line is given by

$$I'_{\omega,2} = \frac{\sinh \gamma l}{Z_0} * V_2 + \cosh \gamma l * \left(I_{\omega,2} + j\omega C_j V_2 \right) \tag{6}$$

Simply by adding up the total incremental dc current and incident power, the current responsivity of twin SIS junctions at frequency ω can now be written

$$R_i(\omega) = \frac{2\left(\Delta I_{dc,1} + \Delta I_{dc,2}\right)}{V_1 \left| I_{\omega,1} + I'_{\omega,2} + j\omega C_j V_1 e^{j\phi} \right|} \tag{7}$$

Obviously, the input impedance of twin SIS junctions is

$$Z_j(\omega) = \frac{V_1 e^{j\phi}}{I_{\omega,1} + I'_{\omega,2} + j\omega C_j V_1 e^{j\phi}} \tag{8}$$

Assuming there is a source impedance Z_s (ω), we obtain the direct-detection response of twin SIS junctions at frequency ω as

$$I(\omega) = \frac{4\,\mathrm{Re}\left(Z_j(\omega)\right) * \mathrm{Re}\left(Z_s(\omega)\right)}{\left| Z_j(\omega) + Z_s(\omega) \right|^2} * R_i(\omega) \tag{9}$$

Based on the direct-detection model established above, we simulated the direct-detection response of the measured twin-junction device. Its source impedance was firstly computed in the frequency range of 0.5-0.9 *THz* with the aid of electromagnetic field simulator named HFSS. Note that the superconducting twin-junction device and the waveguide mount installing the device were both taken into account. The real I-V curve of the twin-junction device was adopted for this simulation. The constant bias potential V0 was assumed to be 2 *mV*, while the reduced signal voltage eV2/hν was given a sufficiently small value (~0.01) so as not to vary the simulated direct-detection response. The simulation result is plotted in Fig.14, together with the measured one. Obviously, they are in good agreement. We also measured the noise performance of the superconducting twin-junction device installed in the same waveguide mount. The result is also shown in Fig.14.

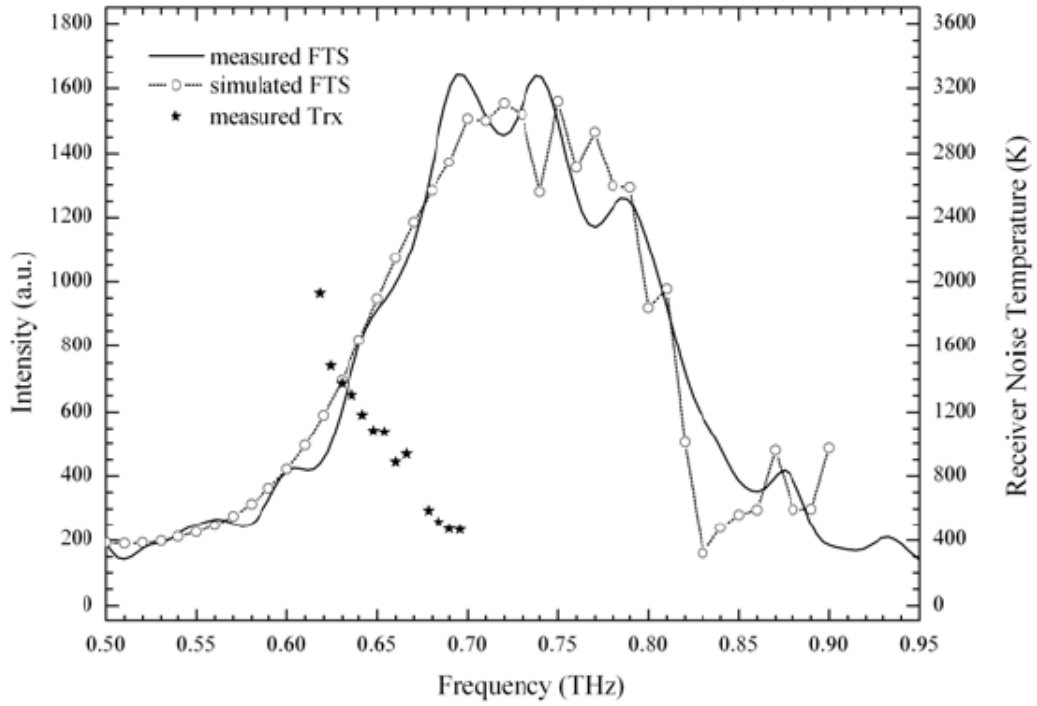

Fig.14 Measured and simulated direct-detection responses, and measured noise temperature of the twin-junction device.

Acknowledgement

The author is grateful to Dr. Terai of National Institute of Information and Communication Technology for valuable comments. I thank Dr. Matsuo of NAOJ for his help in setting the FTS system. This work was supported by NSFC under Contract No. 10673033 and No.10621303.

References

[1] R.J. Ivison, I. Smail, J.-F. Le Borgne, A.W. Blain, J.-P. Kneib, J., Bezecourt, T.H. Kerr, J.K. Davies, "A hyperluous galaxy at z=2.8 found in a deep sub-millimetre survey," *MNRAS*, 298, 583-592. (1998).

[2] J. Zmuidzinasmin and P. L. Richards, *Proc. of the IEEE* 92 1597, (2004).

[3] Frank C. De Lucia, *Optics & Photonics News* 8 44, (2003).

[4] S.P. Huang, J. Li, A.Q. Cao, S.H. Chen, X.F. Shen, Z.H. Lin, S.C. Shi, and J. Yang, "Development of a Compact 500-GHz SIS Receiver," in Proc. of AP-RASC 04, *Tang Keyun and Liu Dayong, Eds. IEEE Press*, 412-413, (2004).

[5] S.C. Shi, T. Noguchi, and J. Inatani, "Analysis of th bandwidth performance of SIS mixers with distributed

junction arrays," in *Proc. 8th Int. Symp. On Space Terahertz Tech.*, Boston, USA, Mar, 81-90, (1997).

[6] Sheng-Cai Shi, Takashi Noguchi, Junji Inatani,Yoshihisa Irimajiri, and Toshimi Saito "Experimental Results of SIS Mixers with Distributed Junction Arrays", *in Proc. of Ninth Int. Symp. On Space Terahertz Tech.*, 223-234, (1998).

[7] A. Karpov, J. Blondel, M. Voss, and K.H. Gundlach, "A three photon noise SIS heterodyne receiver at submillimeter wavelength," *IEEE Trans. Appl. Supercond.*, vol.9, no.2, 4456-4459, (1999).

[8] Z. Wang, A. Kawakami, Y. Uzawa, and B. Komiyama, "NbN/AlN/NbN tunnel junctions fabricated at ambient substrate temperature", *IEEE Trans. appl. Supercond.,* vol .5, no.2, 2322~2325, (1995).

[9] J.R. Gao, M. Hajenius, Z.Q. Yang, J.J. Baselmans, P. Khosropanah, R. Barends and T.M. Klapwijk, "Terahertz superconducting hot electron bolometer heterodyne receivers," *IEEE trans. Applied superconductivity,* vol.17, no.2, 252-258, (2007).

[10] Yu.B. Vachtomin, M.I. Finkel, S.V. Antipov, B.M. Voronov, K. V. Smirnov, N. S. Kaurova, V.N. Drakinski, and G.N. goltsman, "Gain bandwidth of phonon-cooled HEB mixer made of NbN thin film with MgO buffer layer on Si," *13th International Symposium on Space THz Technology,* Harvard University, 259-270, (2002).

[11] H. Ekstron, B.S. Karasik, E.L. Kollberg, and K.S. Yngvesson, "Conversion gain and noise of niobium superconducting hot electron mixer," *IEEE Trans. MTT.* vol.43, no. 4, 938-947, (1995).

[12] Zhang Wen, LiNing, Jiang Ling, Miao Wei, Lin Zhen-Hui, Yao Qiu-Jun, Shi Sheng-Cai, Chen Jian, Wu Pei-Heng, S.I. Svechnikov, Yu.B. Vachtomin, S.V. Antipov, B.M. Voronov and Goltsman, "Noise behavior of a Thz Superconducting hot-electron bolometer mixer," *Chinese physics letter*, vol.24, no.6, 1778-1781, (2007).

[13] B.S. Karasik, A.I. Elantev, "Analysis of the noise performance of a hot-electron bolometer mixer," *6th Int. Symposium on Space Terahertz Technology*, Pasadena, CA, 229-247, (1995).

[14] H. Ekstron, B.S. Karasik, E.L. Kollberg, and K.S. Yngvesson, "Conversion gain and noise of niobium superconducting hot electron mixer," *IEEE Trans. MTT.* vol.43, no.4, 938-947, (1995).

[15] D.F. Filipovic, G.P. Gauthier, S.Raman, and G.M. Rebeiz, "Off-axis properties of silicon and quartz Dielectric lens antennas," *IEEE Trans. AP*. Vol.45, no.5, 760-766, (1997).

[16] C.C. Chin, M.J. Wang, W.L. Shan, W. Zhang, H.W. Cheng, S.C. Shi, and T. Noguchi *Int. J. IR & MM Waves,* 23 731, (2002).

[17] J. R. Tucker, *IEEE Journal of Quantum Electronics,* 15 1234, (1979).